**Electronic Supplementary Information (ESI) for Journal of Materials Chemistry A.**


# Supplementary Material: *An in situ* formed inorganic conductive network enables high stability and rate capability of single-crystalline nickel-rich cathodes

Xi Chen, †[a] Yu Tang, †[b] Zhibo Zhang,[a] Muhammad Ahmad, [a] Iftikhar Hussain, [a] Tianyi Li, [c] Si Lan,[d] Kaili Zhang, *[a] Qi Liu, *[b]

[a] Department of Mechanical Engineering, City University of Hong Kong, Hong Kong 999077, P. R. China

[b] Department of Physics, City University of Hong Kong, Hong Kong 999077, P. R. China

[c] Argonne National Laboratory, X-Ray Science Division, Argonne Illinois 60439, USA

[d] Shenzhen Research Institute, City University of Hong Kong, Shenzhen 518057, P. R. China

†Equal contribution

*Correspondence to: Prof. Kaili Zhang, Email: kaizhang@cityu.edu.hk; and Prof. Qi Liu, Email: qiliu63@cityu.edu.hk

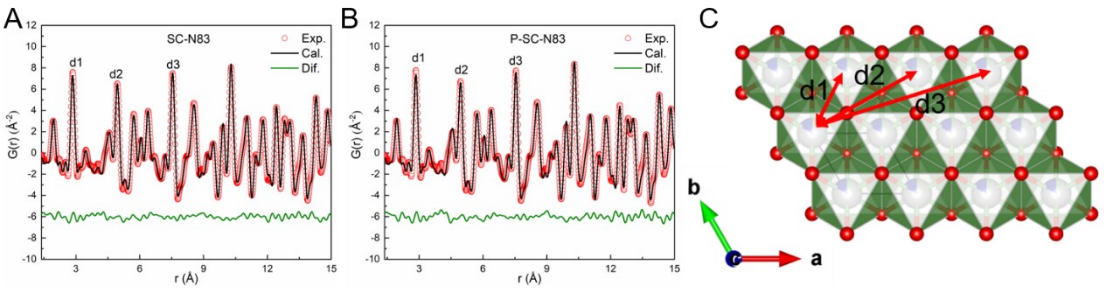


**Supplementary Figure 1.** Full-profile refinement patterns of (a) SC-N83 and (b) P-SC-N83. (c) variation of the three nearest TM-TM distances according to the refinement.

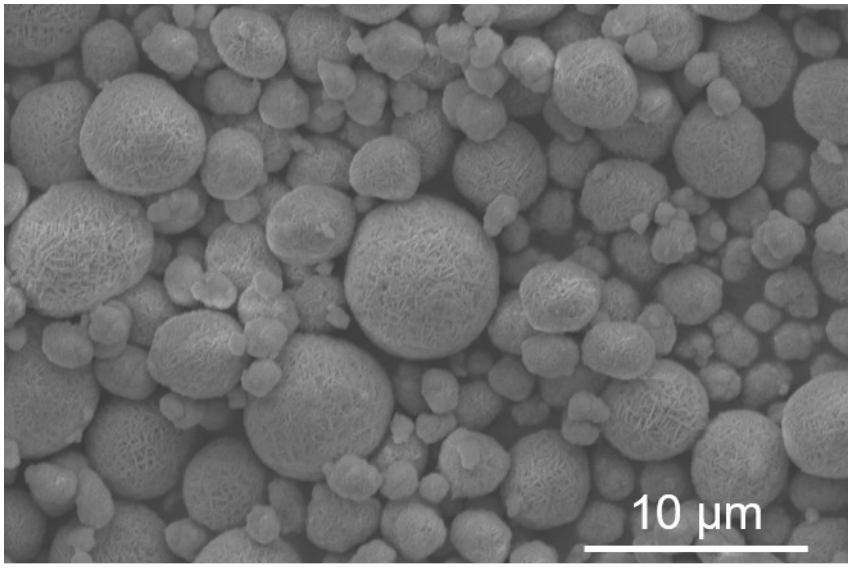


**Supplementary Figure 2.** SEM image of precursor $Ni_{0.83}Co_{0.12}Mn_{0.05}(OH)_2$.

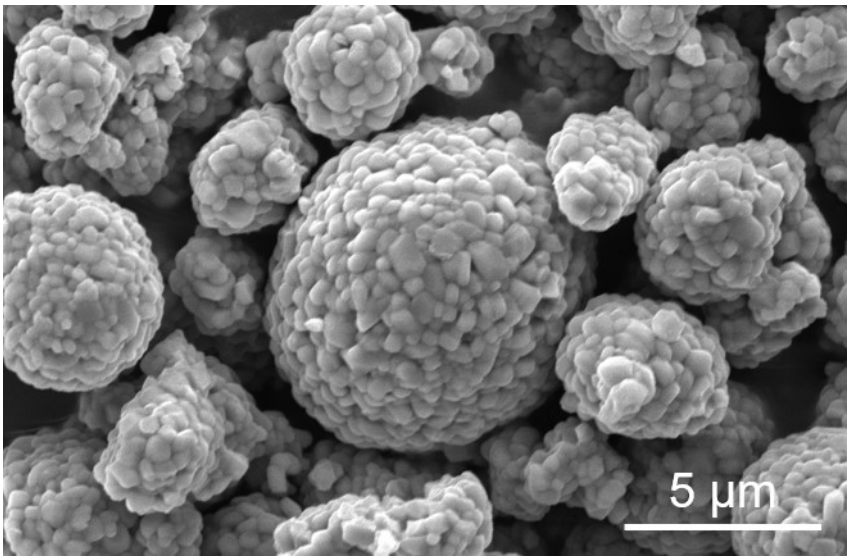


**Supplementary Figure 3.** SEM image of polycrystalline $LiNi_{0.83}Co_{0.12}Mn_{0.5}O_2$ sintered at 800 °C.

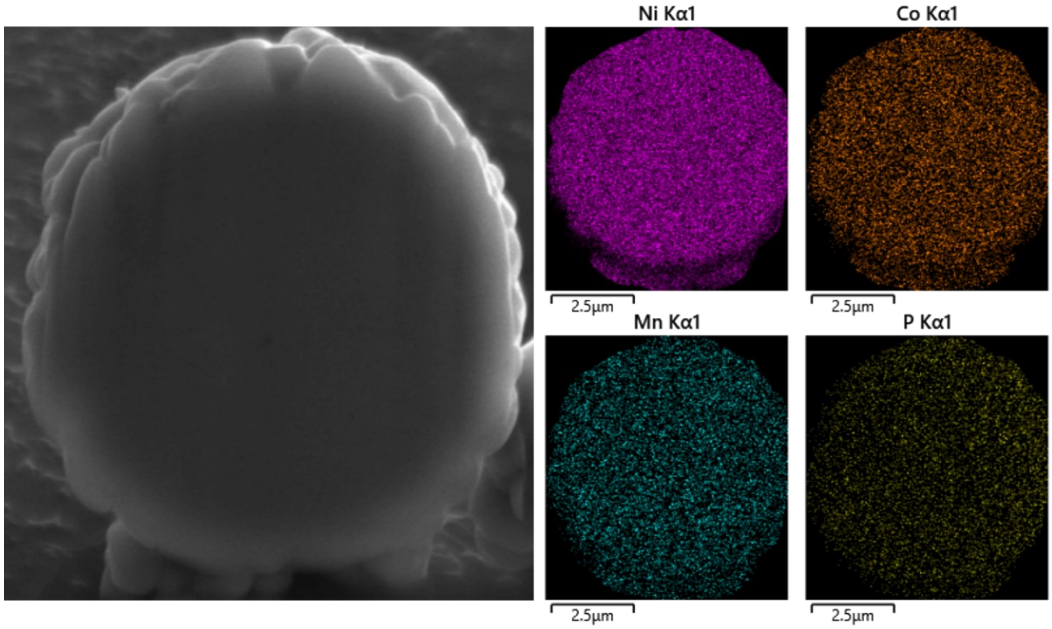


**Supplementary Figure 4.** Cross-sectional elemental distribution of $LiNi_{0.83}Co_{0.12}Mn_{0.5}O_2$ after sintering at 880 °C.

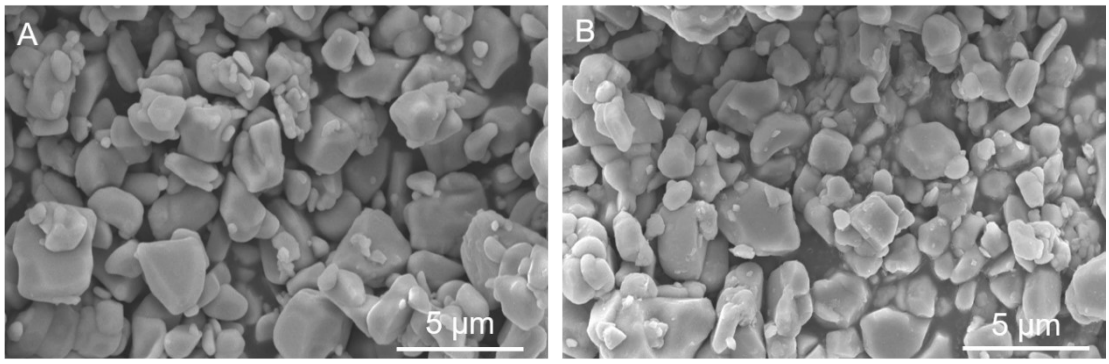


**Supplementary Figure 5.** SEM images of (A) SC-N83 and (B) P-SC-N83 single crystals.

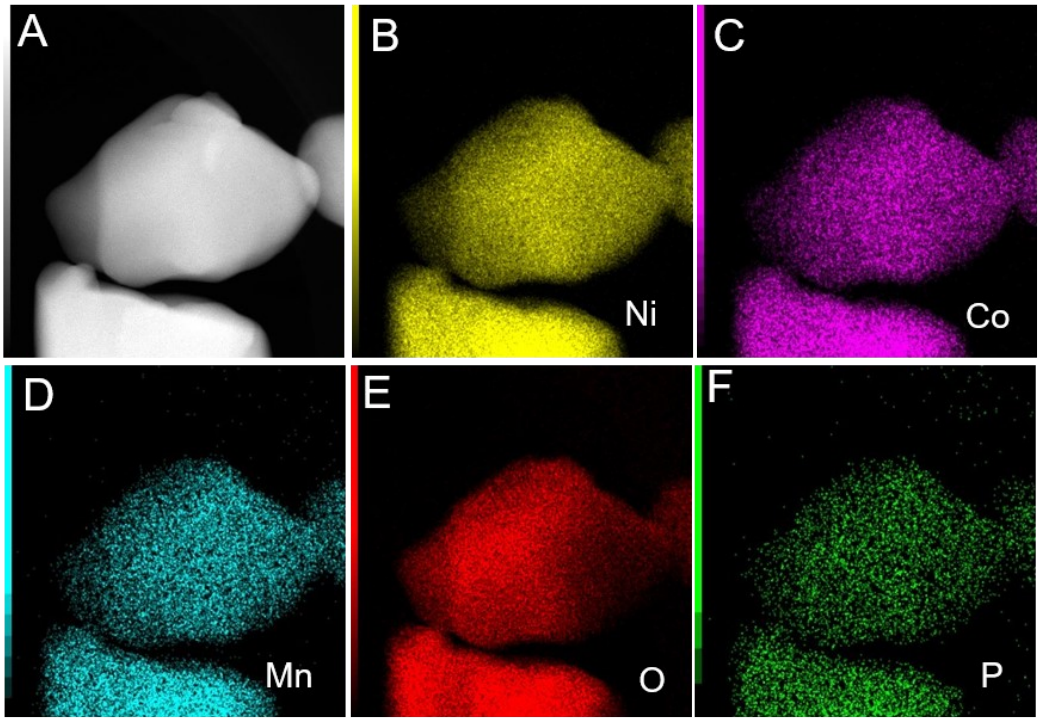


**Supplementary Figure 6.** EDS elemental mapping of Ni, Co, Mn, O, P of P-SC-N83.

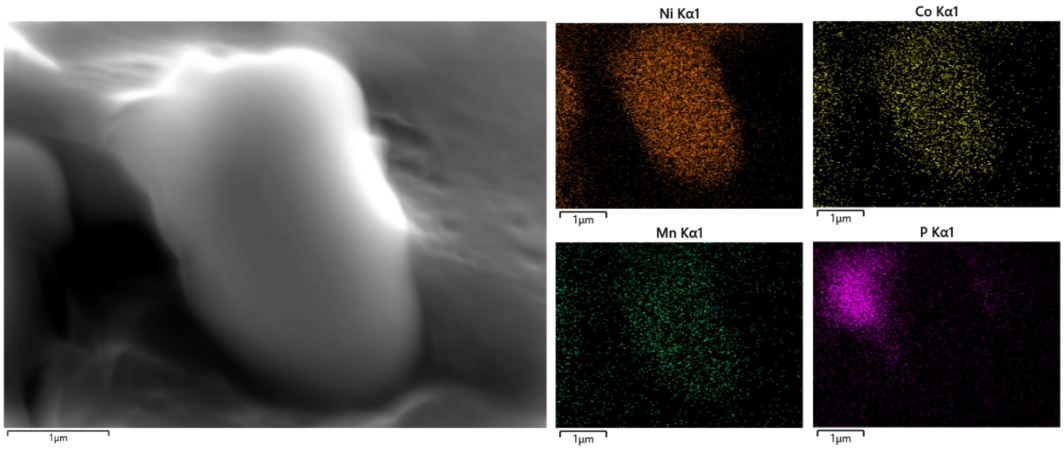


**Supplementary Figure 7.** Cross-sectional elemental distribution of $LiNi_{0.83}Co_{0.12}Mn_{0.5}O_2$ by coating directly on single-crystalline particles after the second calcination.

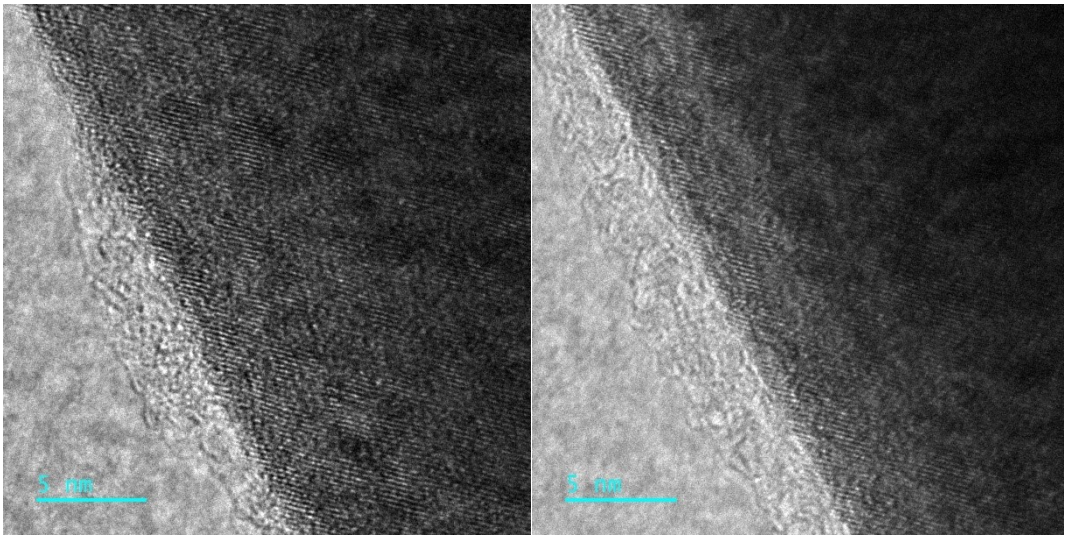


**Supplementary Figure 8.** HR-TEM images of P-SC-N83.

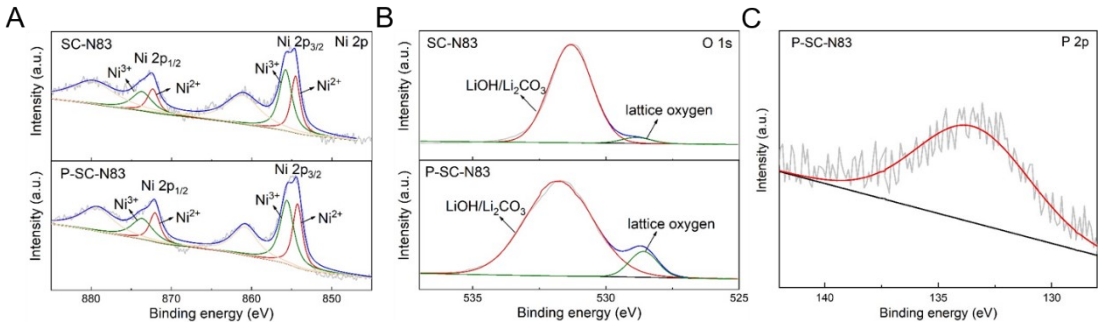


**Supplementary Figure 9.** XPS spectra of (A) Ni 2p, (B) O 1s and (C) P 2p of SC-N83 and P-SC-N83.

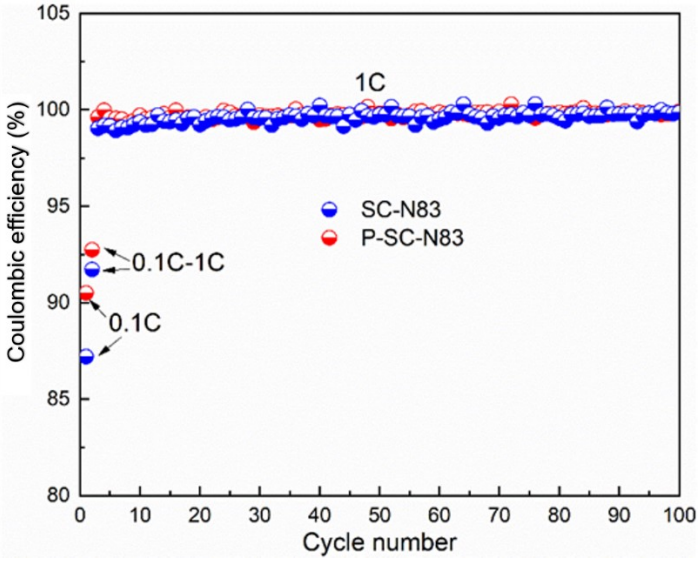


**Supplementary Figure 10.** Coulombic efficiency of SC-N83 and P-SC-N83 in the whole cycling process.

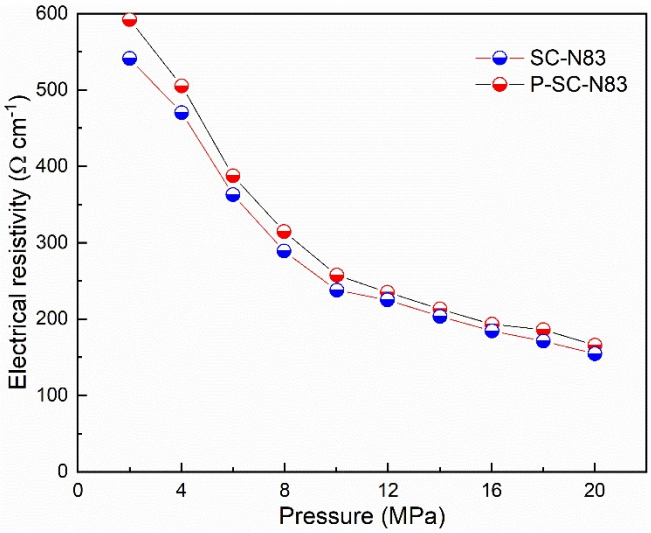


**Supplementary Figure 11.** Powder electrical resistivity of SC-N83 and P-SC-N83 under different pressures.

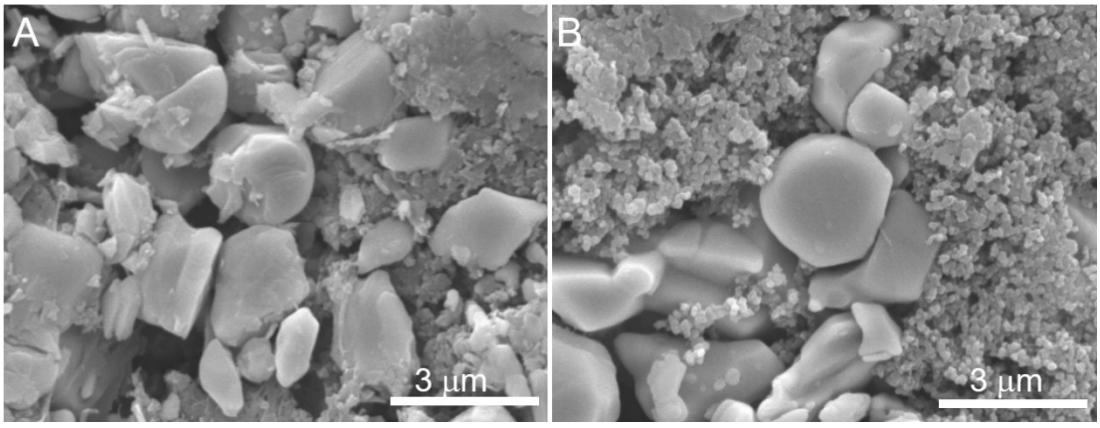


**Supplementary Figure 12.** SEM images of (A) SC-N83 and (B) P-SC-N83 after 100 cycles.

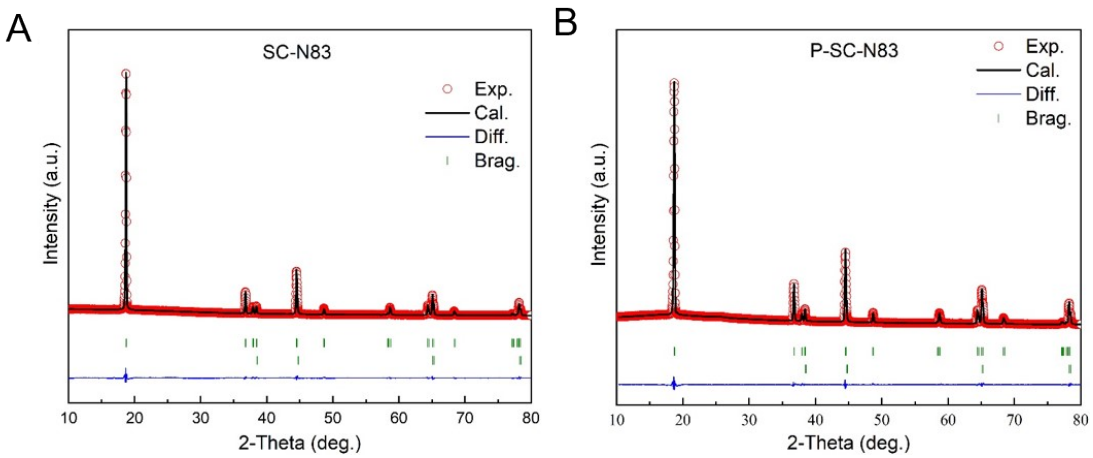


**Supplementary Figure 13.** Full-profile refinement patterns of (A) SC-N83 and (B) P-SC-N83 after 100 cycles.

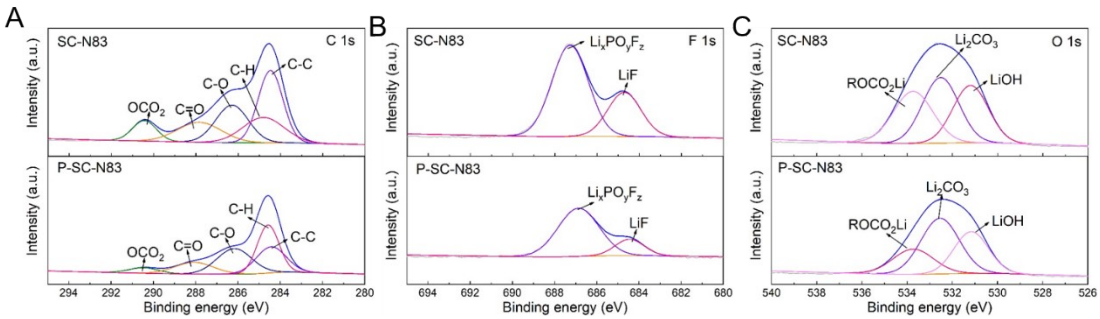


**Supplementary Figure 14.** XPS spectra of (A) C 1S, (B) F 1s and (C) O 1s of SC-N83 and P-SC-N83 after 100 cycles.

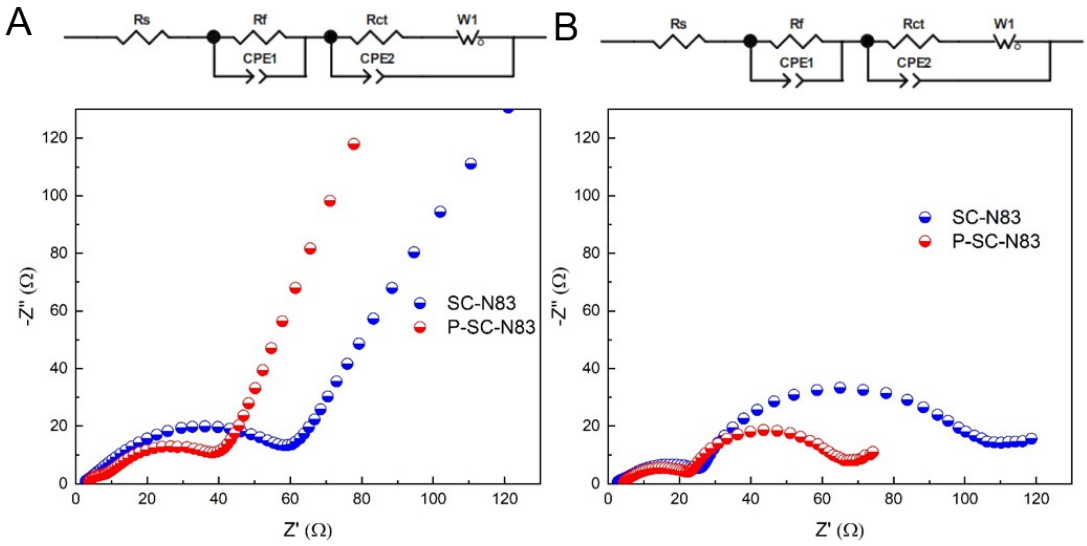


**Supplementary Figure 15.** EIS plots of SC-N83 and P-SC-N83 before (A) and after (B) cycling.

**Supplementary Table 1.** Lattice constants of samples obtained from XRD Rietveld analysis based on the *R*-3*m* space group

| Samples | a-axis (Å) | c-axis (Å) | V (Å$^3$) | Li/Ni disorder | $R_{wp}$ |
|---|---|---|---|---|---|
| SC-N83 | 2.87206 | 14.18912 | 101.362 | 1.27% | 5.1 |
| P-SC-N83 | 2.87778 | 14.20441 | 101.876 | 1.53% | 6.6 |

**Supplementary Table 2.** Lattice constants of samples after 100 cycles obtained from XRD Rietveld analysis based on the *R*-3*m* space group

| Samples | a-axis (Å) | c-axis (Å) | V (Å$^3$) | $R_{wp}$ |
|---|---|---|---|---|
| SC-N83 | 2.86402 | 14.24207 | 101.171 | 6.9 |
| P-SC-N83 | 2.86460 | 14.22557 | 101.095 | 6.2 |

**Supplementary Table 3.** EIS plots fitting results according to the given equivalent circuit.

| Samples | Before cylcing | | After cycling | |
|---|---|---|---|---|
| | $R_f(\Omega)$ | $R_{ct}(\Omega)$ | $R_f(\Omega)$ | $R_{ct}(\Omega)$ |
| SC-N83 | 6.95 | 49.61 | 23.63 | 83.88 |
| P-SC-N83 | 6.84 | 29.19 | 18.75 | 45.29 |